

CHARACTERIZATION OF MERCURY CADMIUM TELLURIDE USING NONDESTRUCTIVE  
TRANSVERSE ACOUSTOELECTRIC VOLTAGE MEASUREMENTS

P. Das, M. Tabib-Azar and Bijan Davari

Elec., Comp. and Systems Engrg. Dept.  
Rensselaer Polytechnic Institute  
Troy, New York 12181

J. H. Everson

Honeywell Electro-Optics Division  
2 Forbes Road  
Lexington, MA 02173

Abstract

$Hg_{1-x}Cd_xTe$  is extensively used today as a versatile infrared detector material with increasing importance in the fabrication of focal plane arrays. In this work  $Hg_{1-x}Cd_xTe$  electronic properties are investigated using nondestructive SAW technique. The transverse acoustoelectric voltage (TAV) is monitored across the  $Hg_{1-x}Cd_xTe$  sample which is placed in proximity of a  $LiNbO_3$  delay line. TAV is developed due to the nonlinear interaction between the electric field accompanying SAW, and the free carriers near the  $Hg_{1-x}Cd_xTe$  surface. Contactless TAV and surface photovoltage spectroscopy are performed to determine the bandgap and thus the alloy composition (x) of  $Hg_{1-x}Cd_xTe$ .

The TAV versus voltage measurements are also performed for further investigation of  $Hg_{1-x}Cd_xTe$  surface properties (such as conductivity type and possible surface inversion due to passivation by ZnS).

Introduction

Full scale production for current and future generation military infrared systems will require linear arrays and mosaic focal planes with a large number of infrared detectors. Mercury cadmium telluride provides a predominant role as the material for these detectors.<sup>1</sup> To maintain high volume photo-detector production and maximum yield for systems such as Advanced FLIR Technology (AFT), Thermal Weapon Sights (TWS) and the Shuttle Infrared Telescope Facility (SIRTF), advanced nondestructive contactless techniques will be needed.

For example, a fast, reliable contactless technique is highly desirable for characterizing semiconductor materials at several key production points before completion of the final photodetector. These points may include annealing, slicing, polishing, etching, surface passivation and implant profiling. Contactless testing provides considerable savings in labor and materials by rejecting a faulty device early during production and by making this determination with relative ease compared with other techniques requiring ohmic contacts or metallization. The contactless technique chosen for this paper uses Surface Acoustic Wave (SAW). Different implementations of the SAW technique<sup>2-10</sup> have been used for semiconductors such as Silicon, Cadmium-Sulphide, Indium Arsenide, Indium Phosphide, Gallium Arsenide and Gallium Phosphide. In this paper, it

is extended to include Cadmium Telluride (CdTe) and Mercury Cadmium Telluride with varying alloy composition ( $Hg_{1-x}Cd_xTe$ ).

The main feature of the SAW technique is that the probing tool is an AC electric field which is generated at the surface of a piezoelectric material and is coupled to the semiconductor surface without any form of contact. To produce this electric field the SAW is generated by applying rf voltage to the interdigital transducers made on the surface of a piezoelectric material ( $LiNbO_3$ )<sup>2,3</sup> as shown in figure 1a. Because  $LiNbO_3$  is piezoelectric, the elastic wave is accompanied by an electric field with a component perpendicular to the surface of the  $LiNbO_3$  substrate (probing field). This component exists outside the  $LiNbO_3$  to a distance of about an acoustic wavelength ( $\approx 31.6 \mu m$  for 110 MHz rf pulse). When the probing electric field reaches under the semiconductor surface (which is placed above the delay line (fig. 1b)), the acousto-electric interaction with the free carriers of the semiconductors manifests itself as attenuation and change in velocity of SAW and the appearance of a d.c. voltage across the semiconductor. The transverse component of this voltage which is called the transverse acoustoelectric voltage (TAV) is the monitored signal throughout the following experiments. The penetration depth of the probing field is on the order of the semiconductor extrinsic Debye length or the acoustic wave length, whichever is shorter. TAV signal can be monitored by placing a metal plate above the semiconductor and another one either below the  $LiNbO_3$  substrate (fig. 1b) or above it (fig. 1d). To monitor the dc TAV signal through the possible insulators, the rf voltage and thus the probing electric field are pulsed. TAV is capacitively coupled to the metal plates, so the presence or absence of insulator layer on the semiconductor surface is immaterial. The nature of these contacts through which the TAV is monitored is important for a nondestructive measurement. In spectroscopy measurements, the configuration of fig. 1b is used where the ground path is an Al plate evaporated underneath the  $LiNbO_3$  and the monochromatic incident beams are shone on the semiconductor surface through a small window. This structure is sufficient for spectroscopic measurements where the modulation of the surface potential by an external dc bias is not needed. On the contrary, if the surface potential has to be modulated, a very large voltage in excess of 1000 volts is needed to sustain the voltage drop across the thick  $LiNbO_3$  substrate ( $\approx 3 mm$ ).<sup>9</sup> To overcome this problem, the new configuration which is shown in fig. 1c is

devised. In this configuration, a thin aluminum structure ( $\approx 1000 \text{ \AA}$ ) is evaporated on the  $\text{LiNbO}_3$  surface which provides the ground path for the TAV signal. At the center of the aluminum structure, a window is made which acts as the interaction region. Under the  $\text{Al}$  covered area the electric field tends to zero while the mechanical wave continues to propagate. Once the mechanical wave reaches the interaction window, the probing electric field is regenerated. The semiconductor under test is placed above the interaction region where the probing electric field penetrates inside the semiconductor and produces the TAV signal (fig. 1d). To change the surface potential a dc voltage is applied across the semiconductor through the same structure used to detect the TAV signal. To complete the circuit an  $\text{Al}$  plate is pressed on the semiconductor back surface and the ground path is the  $\text{Al}$  structure on the surface of  $\text{LiNbO}_3$ . The contact to the surface under study (device side) is of special importance. This contact is simply provided by placing the semiconductor on the  $\text{Al}$  coated  $\text{LiNbO}_3$  (fig. 1d) and there is no processing involved. The ground path on the surface of the  $\text{LiNbO}_3$  has reduced the necessary magnitude of the applied dc voltage by a factor of 100 as compared to the previous work<sup>8</sup> due to the elimination of the voltage drop across the  $\text{LiNbO}_3$ .

In this paper the feasibility of the TAV measurement technique to CdTe and  $\text{Hg}_{1-x}\text{Cd}_x\text{Te}$  is demonstrated using both the spectroscopy and TAV vs applied bias voltage measurements.

#### Transverse Acousto-Electric Voltage and Experimental Procedure

TAV measurements in general, consist of monitoring the TAV amplitude or transient time constants while the semiconductor surface condition is varied by an external excitation such as photons, applied bias field and heating or cooling. TAV amplitude dependence on the electronic properties of the semiconductor surface is described elsewhere<sup>10</sup> and is proportional to the conductivity difference between the electrons and holes.

Fig. 2 shows the plot of TAV vs electron and hole concentration using eqn. (15) of reference 10. The constants used for the figure are shown in Table I and the frequency of SAW assumed is 100 MHz. The form of the curve is similar for other semiconductors. The important features of the plot are: 1) n type surface conductivity exhibits a positive TAV and vice versa for p type. 2) There is a maximum in both the n and p regions. The reason is that for the intrinsic case there are few carriers to interact with the probing electric field and the TAV is very small. As the concentration of the free carriers increases, the TAV grows until it reaches the maximum. At higher conductivities, the free carriers begin to screen the probing electric and the TAV amplitude reduces. Thus by monitoring the TAV amplitude one can distinguish between electron and hole surface conductivities and also obtain the magnitude of the surface conductivity. Because of the large difference in electron and hole mobilities, the peak TAV of n-type samples is much larger than that of p-type. Because of the large bandgap

of CdTe, TAV is predominant only in small regions of electron and hole concentrations. One should note the high sensitivity of the TAV signal at very low carrier concentrations which extends the measurement capability to very high resistivity samples. This is a distinct advantage over other measurement techniques such as Hall voltage and four point probe measurements. On the other hand, the sensitivity of the TAV technique decreases at very high carrier concentration. Lock-in detection of the TAV amplitude has alleviated this problem to some extent.

In the experiments reported here, the rf pulse applied to the input transducer has frequency of 110 MHz (55 MHz is also used) and its amplitude is about 10 volts P/P (50  $\Omega$  load resistance). The pulse duration is in the range of  $\mu\text{sec}$ . with repetition rate of about 30 Hz. The TAV amplitude is measured by a lock-in amplifier locked to the envelope of the rf excitation pulse. In some cases the TAV amplitude is recorded manually.

Fig. 3 shows a typical input and output of the SAW delay line and the resulting TAV when HgCdTe is used. In this picture trace (a) is the 110 MHz input rf pulse with about 2.5  $\mu\text{sec}$ . Trace (c) shows the TAV signal obtained from the HgCdTe sample which is about 7  $\mu\text{sec}$  delayed with respect to the input rf pulse. The first peak in trace (c) with no delay (the small peak) is due to the radiation from rf input pulse.

The time constant associated with the leading edge of the TAV signal can be related to the generation lifetime ( $\tau_g$ ) and surface generation velocity ( $S_g$ ).<sup>6</sup> The separation of  $\tau_g$  and  $S_g$  is possible by the application of a depleting dc bias field across the semiconductor.<sup>7</sup>  $\tau_g$  and  $S_g$  are determined for silicon wafers (used for VLSI fabrication) as an indication of the defect density. These parameters can be depth profiled by the new technique introduced in reference 5. However, these experiments have not been performed as yet for CdTe or HgCdTe samples.

Spectroscopy of TAV amplitude is used to reveal the subbandgap absorption and the interface states energy band structure of the semiconductors. In this method, the wavelength of the incident beam is scanned in the desired range. The detection sensitivity of the subbandgap structures can be enhanced by two beam spectroscopy as compared to one beam, by the proper choice of the bias light wavelength.

The monochromatic incident beam is chopped with a mechanical chopper which also provides the reference signal for the lock-in amplifier and the pulse generator. Bausch & Lomb monochromator (B & L Cat. #33-86-25 with high intensity tungsten source) is used for the wavelengths in the range of 500 to 3000 nm. The TAV amplitude is recorded and plotted against the wavelength. To obtain the desired wavelength range, three gratings are used covering (500-750 nm), (700-1150 nm) and (1150-3000 nm) ranges. The incident photon flux is kept constant up to 2100 nm (by experimental

calibration using a thermopile) and is  $7 \times 10^{14}/\text{cm}^2$  sec. For the wavelengths higher than 2100 nm the monochromator output is not experimentally calibrated and only the spectral flux output curve, furnished by the manufacturer, is used (for grating 33-86-04). This spectral flux exhibits a strong decrease of the output power for wavelengths beyond 2750 nm. A high resolution HRS-2 (Jobin Yvon) monochromator with 300 grooves/mm grating is also used in the spectral range from 1600 to 3200 nm. The resolution of these measurements is about  $125 \text{ \AA}$  (lowest resolution is used to obtain a higher output flux).

TAV measurements under the applied dc bias (which modulates the surface potential and the depletion width) are of great importance. Both TAV amplitude and transient time constant dependence on the bias voltage (TAV-V and  $\tau$ -V) are utilized. In these experiments the new delay line structure (fig. 1c,d) is used. TAV-V plots can be used as a nondestructive alternative to C-V measurements in order to determine the oxide charge and flat band voltage of thermally oxidized silicon wafers.<sup>2</sup> A new profiling technique is devised which is applicable to the measurements which are primarily sensitive to the free carrier concentration rather than the depletion layer thickness.<sup>5</sup> By using this technique and the TAV-V plots, the free carrier concentration depth profile can be obtained<sup>5</sup> similar to the differential capacitance methods. In the TAV-V experiments, the first harmonic of the TAV signal which is directly proportional to the TAV amplitude is monitored by a lock-in amplifier. The external bias voltage is scanned over the desired range (typical range  $\approx \pm 10$  volts) and the TAV-V is recorded. The operation is simple and there is no need to fabricate any form of contact (e.g., MOS, pn, or Schottky barrier) to the semiconductor surface. The time constants associated with the TAV transients are monitored under the applied bias voltage<sup>7</sup> in order to determine the generation lifetime ( $\tau_g$ ) and surface generation velocity ( $S_g$ ). Using the TAV-V and  $\tau$ -V plots simultaneously, the position of the recombination center within the semiconductor bandgap can be determined.<sup>7</sup>

#### Results and Discussion

The properties of the samples used for different experiments are listed in Table II. Sample A is  $\text{Hg}_{1-x}\text{Cd}_x\text{Te}$  with  $x = 0.4$ . No special surface passivation was performed for this sample. Sample B has a  $3500 \text{ \AA}$  thick zinc sulphide passivation layer. Sample C is CdTe and is included in the study as CdTe is often used as the substrate material for growing HgCdTe by liquid phase epitaxy.

#### TAV Spectroscopy

TAV and photo-voltage spectra for Sample A are similar and shown in figure 4. The spectrum is used to estimate the bandgap and thus the alloy composition ( $x$ ) of the HgCdTe sample. Figure 3 shows that for wavelengths higher than 2000 nm there is a strong minimum around 2350 nm and also the response falls off sharply for wavelengths higher than 2500 nm. Minimum around 2350 nm is partially attributed to the monochromator spectral flux and

partly to the sample's optical characteristic. The wavelength corresponding to the half peak value of the spectral response (the cut off wavelength,  $\lambda_{CO}$ ) is about 2500 nm or  $2.5 \mu\text{m}$ . Thus the bandgap can be estimated to be about:

$$E_g \approx \frac{1.24}{2.5} = 0.5 \text{ eV} .$$

The corresponding alloy composition ( $x$ ) is estimated by linear interpolation of the data presented in ref. 1 and it is about 0.44 which is in reasonable agreement with the value obtained by density measurements. The presence of discrete defect levels at HgCdTe surface influences the spectra and might explain the rest of the structures. However, to pinpoint their effect, one needs to perform the two beam spectroscopy which has not yet been performed.

#### TAV-V Measurement

In Figs. 5, 6, and 7 the TAV-V plots are given for Samples A, B and C respectively. TAV polarity is negative at zero bias voltage (sample A) indicating a p type surface conductivity. In HgCdTe semiconductor the electron mobility is about 100 times higher than the hole mobility. Since the TAV signal is related to the conductivity difference between electron and holes, it is possible to obtain positive TAV polarity even if the electron concentration is about 100 times less than hole concentration. By applying a positive D.C. voltage to the HgCdTe surface, the electron conductivity increases (due to the increase in the surface electron concentration) and the negative TAV amplitude decreases. For further increase in voltage, the surface conductivity changes from p to n type, and at around .15V the TAV is zero and then the TAV polarity is reversed to positive sign (indication of n type surface conductivity). It should be noted that in fig. 5 the horizontal coordinate is the value of the applied D.C. voltage across the HgCdTe (fig. 1(c)). In the negative direction, the holes increase due to accumulation. TAV initially increases in the negative direction, reaches a peak at -0.1V and by further increase of the voltage in the negative direction, it decreases due to the screening effect of the holes. Curves similar to fig. 5 have been obtained for many samples. In all the figures, the shape of the curve remains more or less the same although the voltage axis is shifted indicating a different flatband potential and possible different contaminant charges on the semiconductor surface. C-V measurements on similar samples also show this change in the surface charge density for unpassivated surfaces.

Fig. 6 shows the TAV-V for ZnS passivated HgCdTe sample. Comparing figs. 5 and 6 we note that there is a shift of  $(-0.8 - (+0.15)) = .95\text{V}$  in the applied voltage at the TAV zero crossing which is due to the change of the flatband potential between the passivated and bare samples. TAV vs V also has rather sharp peaks and valleys. Preliminary time constant measurements also show similar peaks and valleys at the proper applied voltages as shown in the figure. This behavior can be explained by postulating the presence of defect levels within

the bandgap. Another explanation might be due to the strong hysteresis effect which is also observed in the C-V curves of passivated samples. Thus the data might point to the fact that proper equilibrium was not reached in the measurement. However, further detailed measurements are needed before any definite conclusions can be drawn.

Fig. 7 shows the TAV-V data for CdTe. At zero bias it is positive and increases dramatically for positive bias. However, for negative bias, very little change is observed. Noting the shape of TAV vs carrier concentration in fig. 2(c), one can conjecture that the sample is p-type and tends to get inverted with positive voltage.

As discussed in ref. 2, from TAV-V plots using analytical modes and numerical computations, one can infer the flat-band potential and the equivalent interface charge density at the surface of the interface. However, this has not yet been performed.

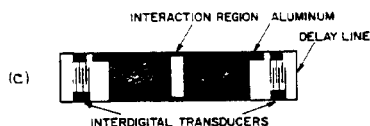
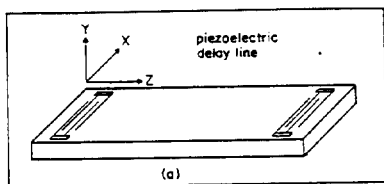
In conclusion, the SAW nondestructive surface and interface characterization technique has been applied to CdTe and HgCdTe. The study shows that useful characterization is feasible although there is much to be performed before it becomes useful for production of devices such as focal plane arrays.

#### Acknowledgement

It is a pleasure to acknowledge the contribution of Dr. Peter Zimmermann of Honeywell Electro-Optics Division, through many discussions and sample preparations.

TABLE I

	Hg <sub>0.6</sub> Cd <sub>0.4</sub> Te		CdTe
	T = 77°K	T = 300°K	T = 300°K
Energy gap	0.40	0.433	1.56
Intrinsic carrier concentration	6x10 <sup>10</sup>	6x10 <sup>14</sup>	10 <sup>7</sup>
Electron Mobility	5x10 <sup>3</sup>	3x10 <sup>3</sup>	1000
Hole Mobility	200	100	100
Dielectric constant	15	15	10.3



#### References

1. M. Reine, A. K. Sood and T. J. Tredwell, "Photovoltaic Infrared Detectors" in "Mercury Cadmium Telluride", Vol. 18 of Semiconductors and Semimetals, edited by R. K. Williardson and A. C. Beer, Academic Press, NY, (1981).
2. B. Davari, P. Das and R. Bharat, J. Appl. Phys. 54, pp. 415 (1983).
3. B. Davari and P. Das, J. Appl. Phys. 53, pp. 3668 (1982).
4. B. Davari and P. Das, Appl. Phys. Lett. 40, pp. 807 (1982).
5. B. Davari and P. Das, IEEE Trans. Electron Device Letters, EDL-4, No. 6, pp. 169 (1983).
6. B. Davari, P. Das, K. Yang and W. A. Westdorp, IEEE International Electron Devices Meeting (IEDM), IEEE Cat. 82CH 1832-5, pp. 66 (1982).
7. B. Davari, M. Tabib-Azar, K. I. Lee, P. Das, E. Mendel and D. A. Miller, to be presented at IEEE International Electron Devices Meeting (IEDM) to be held at Washington, DC, Dec. 1983.
8. H. Gilboa and P. Das, IEEE Trans. Electron Devices, ED-27, pp. 461 (1980).
9. P. Das, R. T. Webster and B. Davari, Appl. Phys. Lett. 34, pp. 307 (1979).
10. P. Das, M. K. Roy, R. T. Webster and K. Varahramyan, IEEE Ultrasonic Symposium Proceedings, pp. 278, Sept. (1979).

TABLE II

Sample #	Hg <sub>1-x</sub> Cd <sub>x</sub> Te	Passivation	N <sub>A</sub> (cm <sup>-3</sup> )	Hole Mobility $\frac{cm^2}{V \cdot sec}$
A	x = .4	No	-	100
B	x = .45	1500 Å Zinc Sulphide	~ 7.8x10 <sup>16</sup>	54.8
C	x = 1	No	2x10 <sup>15</sup>	100

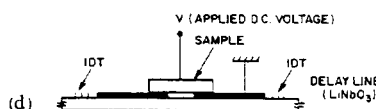
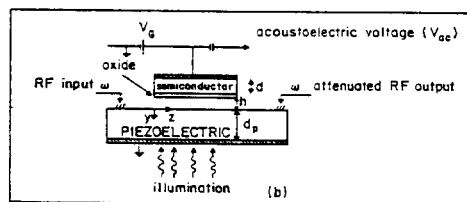
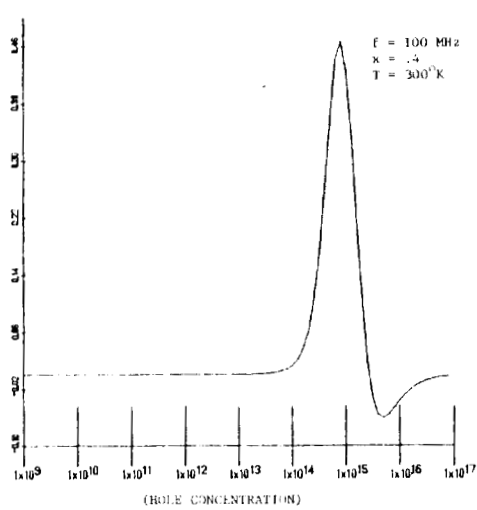
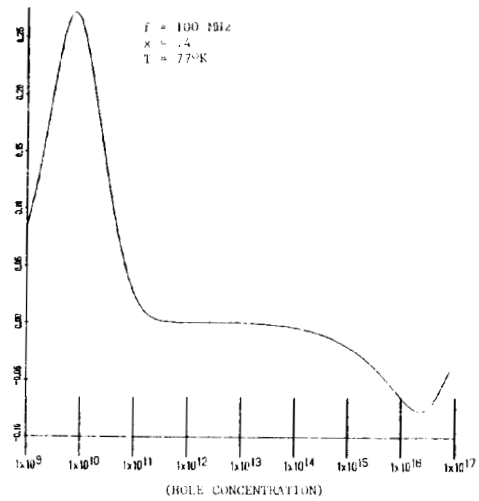


Fig. 1 Delay line structures used in TAV measurements

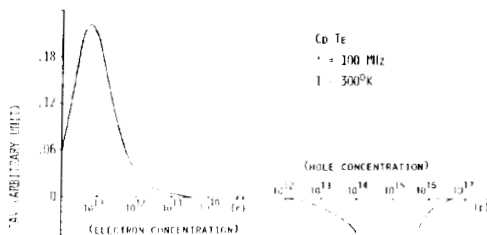


(a)



(b)

Fig. 2 Theoretical plot of TAV vs electron, hole concentration. a)  $\text{Hg}_{1-x}\text{Cd}_x\text{Te}$  ( $x = 0.4$ ) at  $300^\circ\text{K}$ , b)  $\text{Hg}_{1-x}\text{Cd}_x\text{Te}$  ( $x = 0.4$ ) at  $77^\circ\text{K}$ , c)  $\text{CdTe}$  at  $300^\circ\text{K}$



(c)

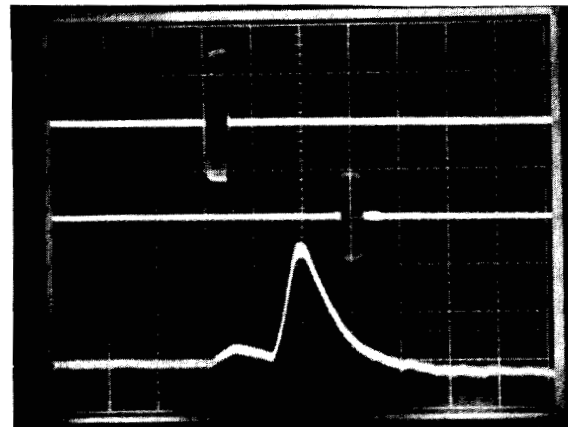


Fig. 3 RF pulse input, output and TAV waveforms; Trace (a): Input RF pulse, frequency =  $110 \text{ MHz}$ , vertical scale =  $5 \text{ V/div.}$ , horizontal scale =  $5 \text{ } \mu\text{sec/div.}$ , trace (b): output RF pulse, vertical scale =  $0.5 \text{ V/div.}$ , trace (c): TAV signal, vertical scale =  $1 \text{ mV/div.}$ , horizontal scale =  $5 \text{ } \mu\text{sec./div.}$

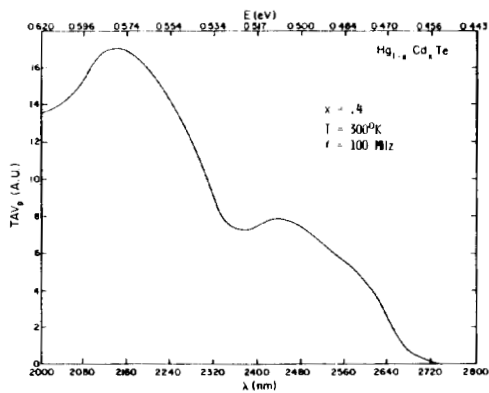


Fig. 4 TAV spectrum for Sample A

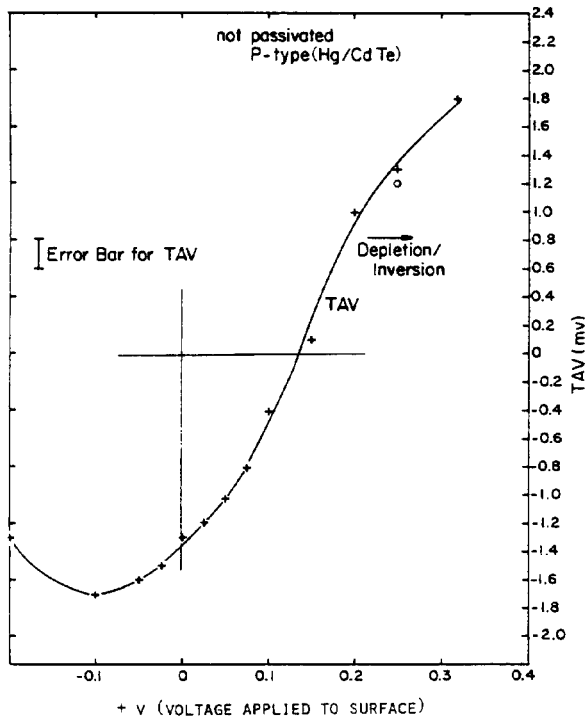


Fig. 5 TAV-V curve for  $Hg_{.6}Cd_{.4}$  at  $T = 300^{\circ}K$ ,  $f = 100$  MHz

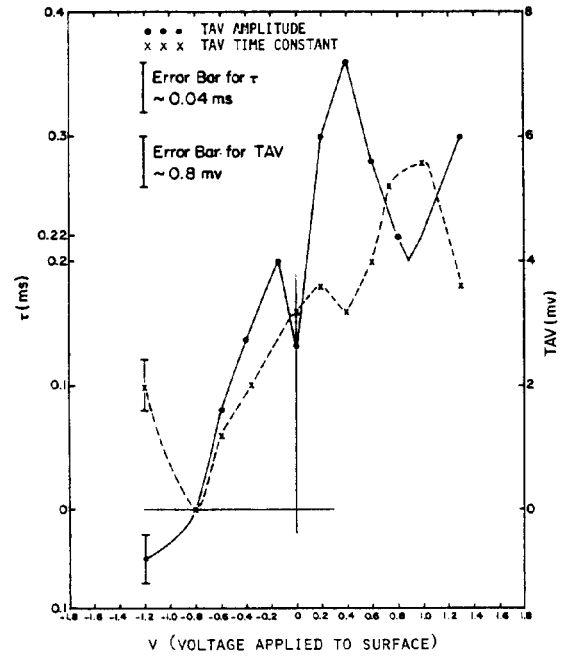


Fig. 6 TAV-V curve for  $Hg_{.55}Cd_{.45}Te/ZnS$  at  $T = 300^{\circ}K$ ,  $f = 100$  MHz

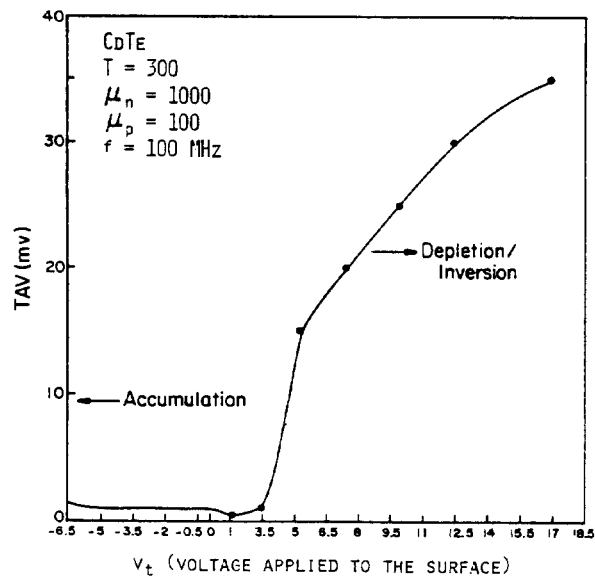


Fig. 7 TAV-V curve for CdTe at  $T = 300^{\circ}K$ ,  $f = 300$  MHz